The Journal of Experimental Biology 210, 2453-2463
Published by The Company of Biologists 2007
doi:10.1242/jeb.003343

Electron and ion microprobe analysis of calcium distribution and transport in coral tissues

Alan T. Marshall[1,*], Peta L. Clode[2], Robert Russell[3], Kathryn Prince[3] and Richard Stern[2,†]

[1]*Analytical Electron Microscopy Laboratory, Faculty of Science, Technology and Engineering, La Trobe University, Melbourne, VI 3086, Australia,* [2]*Centre for Microscopy, Characterisation and Microanalysis (M010), The University of Western Australia, 35 Stirling Hwy, Crawley, WA 6009, Australia and* [3]*SIMS Laboratory, ANSTO, New Illawara Road, Lucas Heights, NSW 2234, Australia*

*Author for correspondence (e-mail: A.Marshall@latrobe.edu.au)

†Present address: GA Geochronology Laboratory, Minerals Division, Geoscience Australia, Canberra, ACT 2601, Australia

Accepted 24 April 2007

Summary

It is shown by x-ray microanalysis that a gradient of total intracellular Ca concentration exists from the outer oral ectoderm to the inner skeletogenic calicoblastic ectoderm in the coral *Galaxea fascicularis*. This suggests an increase in intracellular Ca stores in relation to calcification. Furthermore, Ca concentration in the fluid-filled space of the extrathecal coelenteron is approximately twice as high as in the surrounding seawater and higher than in the mucus-containing seawater layer on the exterior of the oral ectoderm. This is indicative of active Ca^{2+} transport across the oral epithelium. Polyps were incubated in artificial seawater in which all ^{40}Ca was replaced by ^{44}Ca. Imaging Ca^{2+} transport across the epithelia by secondary ion mass spectroscopy (SIMS) using ^{44}Ca as a tracer showed that Ca^{2+} rapidly entered the cells of the oral epithelium and that ^{44}Ca reached higher concentrations in the mesogloea and extrathecal coelenteron than in the external seawater layer. Very little Ca^{2+} was exchanged in the mucocytes, cnidocytes or zooxanthellae. These observations again suggest that Ca^{2+} transport is active and transcellular and also indicate a hitherto unsuspected role in Ca^{2+} transport for the mesogloea.

Key words: biomineralisation, coral, calcium, ion microprobe, SIMS, ion transport, x-ray microanalysis.

Introduction

Calcium is involved in numerous cellular functions and, in the ionised state, is usually maintained at an intracellular concentration of less than 1 $\mu mol\ l^{-1}$ within the cytosol. The majority of intracellular Ca is probably bound to calcium-binding proteins and sequestered in intracellular compartments such as the endoplasmic reticulum (Pozzan et al., 1994). Although much is known about calcium signalling (Brini and Carafoli, 2000) and membrane transport systems for calcium (Hoenderop et al., 2005), there is a paucity of information on intracellular Ca transport in relation to calcification and biomineralisation. Relatively little information is available on total intracellular Ca concentrations in skeletogenic tissues even though it may be expected that intracellular Ca concentration would be related to skeletal Ca deposition (e.g. Bordat et al., 2004).

Scleractinian corals form calcium carbonate skeletons and show extremely high rates of skeletal deposition and calcium transport. The processes involved in the formation of the $CaCO_3$ skeleton are not well understood (Cohen and McConnaughy, 2003; Allemand et al., 2004). The nature of the organism (essentially four cell layers closely overlying a massive exoskeleton) renders obtaining physiological information difficult. Investigations of calcification in corals using metabolic and enzyme inhibitors (Marshall, 1996; Tambutté et al., 1996) have indicated the involvement of active Ca^{2+} transport in coral epithelia. It is generally accepted that active Ca^{2+} transport occurs in the aboral epithelia immediately adjacent to the skeleton (McConnaughey, 1994). However, the mechanism of Ca^{2+} transport across the outer, or oral, epithelium is controversial, being reported as active (Wright and Marshall, 1991; Clode and Marshall, 2002a) and passive (Benazet-Tambutte et al., 1996).

Intracellular Ca concentrations have been obtained from tissues of coral larvae by electron microprobe (x-ray microanalysis) (Clode and Marshall, 2004) and we have applied this method in the present investigation to mature coral polyps. As shown in settled coral larvae by Clode and Marshall (Clode and Marshall, 2004), we show that in mature polyps intracellular total Ca is very high and increases from the outer to inner cell layers. We have also used the ion microprobe at low and high spatial resolution (see Guerquin-Kern et al., 2005; Lechene et al., 2006; Clode et al., 2007) to follow the transport of Ca^{2+} across coral epithelia using the stable isotope ^{44}Ca as

a tracer. With ^{44}Ca in the external seawater it was possible to follow the exchange of ^{44}Ca for the endogenous ^{40}Ca in cells and seawater-filled compartments. This allowed direct visualisation of Ca^{2+} influx across epithelia and into the external coelenteron, i.e. the seawater-filled compartment between the oral and aboral epithelia. Our observations are consistent with the suggestion that Ca^{2+} accumulates across the oral epithelium against a concentration gradient and that Ca^{2+} transport is transcellular and involves some sort of active process.

Materials and methods

Coral samples

Colonies of *Galaxea fascicularis* L. were collected from the reef flat at Heron Reef, Great Barrier Reef, Australia and transported in buckets of seawater (SW) to Heron Island Research Station. Colonies were maintained in semi-shaded outdoor flow-through aquaria [photosynthetic photon flux density (PPFD) 500–1500 mmol photons s^{-1} m^{-1}; 23–25°C] and allowed to recover for 2 days. Polyps were easily separated using forceps and placed in trays of running SW (PPFD 50–150 mmol photons s^{-1} m^{-1}; 23–25°C) to recover for a further 2 days. Small separated polyps were incubated for 2 h in jars containing 200 ml filtered SW (0.25 mm) that were partially submerged in shallow, flow-through aquaria in full sunlight (PPFD 800–1900 mmol photons s^{-1} m^{-1}; 23–25°C). Polyps destined for secondary ion mass spectrometry (SIMS) analysis were incubated in vials containing 10 ml of artificial seawater (ASW) (Benazet-Tambutté et al., 1996) in which $^{44}CaHCO_3$ replaced $^{40}CaHCO_3$. Incubation was carried out under the same conditions of light and temperature for 1 min or 8 min. Polyps were then frozen at approximately midday in liquid propane (–190°C) that had been cooled by liquid nitrogen (LN_2), as previously described (Marshall and Wright, 1991). Polyps were gently blotted on seawater-soaked filter paper to remove excess adhering seawater prior to freezing. This was necessary to achieve reasonable freezing rates to minimize intracellular ice crystal damage. All samples were transferred to La Trobe University, Melbourne, in a CryoPak dry shipper (Taylor-Wharton Australia Pty Ltd, Albury, Australia) at –180°C and stored in LN_2 until required.

X-ray microanalysis

For quantitative x-ray microanalysis, frozen polyps were freeze-substituted in 10% acrolein in diethyl ether, essentially as described by Marshall (Marshall, 1980) and Marshall and Wright (Marshall and Wright, 1991), infiltrated in increasing concentrations of ether and Araldite™ mixtures and embedded in Araldite™. Araldite™ was the preferred embedding medium as it contains negligible levels of elements detectable by energy dispersive spectrometry (Pålsgård et al., 1994). All solutions were anhydrous, with processing conducted in a dry box at a relative humidity of 10%. The embedded polyps were cut into slices approximately 0.5 mm thick with a diamond saw (Buehler Ltd, Lake Bluff, IL, USA). Embedded tissue was dissected from the skeleton and re-embedded under anhydrous conditions. Dry cut sections 1.5 μm thick were mounted on Formvar®-filmed copper grids, coated in 100 Å aluminium and analysed by energy dispersive spectrometry. Briefly, x-ray mapping was performed using a JEOL 1200EX analytical scanning transmission electron microscope (STEM) (JEOL Australasia Pty Ltd, Sydney, Australia) with a Link Atmospheric Thin Window energy dispersive detector (Oxford Instruments, High Wycombe, UK). The detector was interfaced to a 4pi Spectral Engine (4pi Analysis Inc., Durham, NC, USA) and a Quadra 700 Apple Macintosh computer. The microscope was fitted with custom-made LN_2-cooled anticontaminators and a LaB_6 filament. Analyses were carried out by elemental imaging using the multispectral analysis program ImagNspect (Ingram et al., 1999), at 120 kV with a beam diameter of <90 nm and a beam current of 5×10^{-10} A. Peak integral and quantitative images were obtained with a resolution of 128×128 pixels and a dwell time of 3 s $pixel^{-1}$. Quantitative numerical data, based upon the Hall peak/continuum model (Hall and Gupta, 1979), were extracted directly from the elemental maps by selecting areas of interest. Individual spectra for each pixel in the selected regions were summed and processed to yield concentrations for every element (LeFurgey et al., 1992). Elemental concentrations are given in mmol kg^{-1} embedded tissue.

Ion microprobe (SIMS) analysis

For analysis by ion microprobe (SIMS) 1–2 μm-thick dry cut sections were flattened on thin aluminium discs and coated with a thin layer of gold. Analysis was carried out in either a Cameca ims5f SIMS (Cameca, Gernevilliers-Cedex, France) operated in the microprobe mode using a duoplasmatron source (oxygen primary ion beam) at 15 kV and 0.5 nA beam current or a Cameca NanoSIMS (Cameca N50). The imaging spatial resolution of the ims5f was <2 μm while the resolution of the N50 is approximately 200 nm. All NanoSIMS analyses were conducted using a 16 kV $16O^-$ primary beam with a probe current of approximately 5 pA (D1-5) to 23 pA (D1-3). Ion maps were acquired at a resolution of 512×512 pixels, with a typical dwell time of between 3 and 7 ms $pixel^{-1}$.

Isotopic images of masses 12, 23, 24, 39, 40, 44 and 88 were recorded to reveal cell and tissue distributions of ^{12}C, ^{23}Na, ^{24}Mg, ^{39}K, ^{40}Ca, ^{44}Ca and ^{88}Sr, respectively. The purity of secondary ion signals was over 90%.

Data processing

Elemental isotope images were processed using ImageJ (http://rsb.info.nih.gov/ij/) to obtain $^{44}Ca/^{40}Ca$ ratios, line scans and pixel intensities of selected regions. Statistical analysis of pixel intensities was carried out by nonparametric tests using the computer program JMP (SAS Institute Inc., Cary, NC, USA). Statistical analysis of calcium concentrations obtained by x-ray microanalysis was carried out by a one-way analysis of variance (ANOVA) with *post hoc* Tukey-Kramer HSD tests using JMP.

Results

Light microscopy

All x-ray and ion microprobe (SIMS) analyses were carried out on 1–2 μm-thick sections of tissues that covered the external wall or theca of the polyp. These tissues can be seen in thick (1 mm) transverse slices of freeze-substituted polyps (Fig. 1A) and visualised in more detail by fluorescence microscopy of slices stained with Acridine Orange (Fig. 1B). The oral epithelia, consisting of oral ectoderm and oral gastrodermis, are well defined. Numerous orange-staining mucocytes are present in both cell layers and numerous yellow-staining symbiotic algae (zooxanthellae) are present in the gastrodermis. The aboral epithelia are much thinner and are hard to distinguish in dissected thin-sectioned preparations for x-ray microanalysis and ion microprobe analysis. Further structural details are apparent in confocal images of slices (Fig. 2A,B). The oral ectoderm comprises non-specialised ectodermal cells, mucocytes and cnidocytes. This is separated from the oral gastrodermis by a well-defined acellular mesogloea. The oral gastrodermis consists of non-specialised gastrodermis cells, mucocytes and host cells containing symbiotic algae (zooxanthellae). The aboral gastrodermis contains relatively few zooxanthellae and consists primarily of non-specialised gastrodermis cells and mucocytes. A thin mesogloea separates the aboral gastrodermis from the tenuous calicoblastic ectoderm that closely adheres to the skeleton. The aboral gastrodermis contains few zooxanthellae and consists primarily of mucocytes and non-specialised gastrodermis cells. The calicoblastic ectoderm is a thin epithelium containing some mucocytes but is primarily composed of skeletogenic cells containing numerous vesicles.

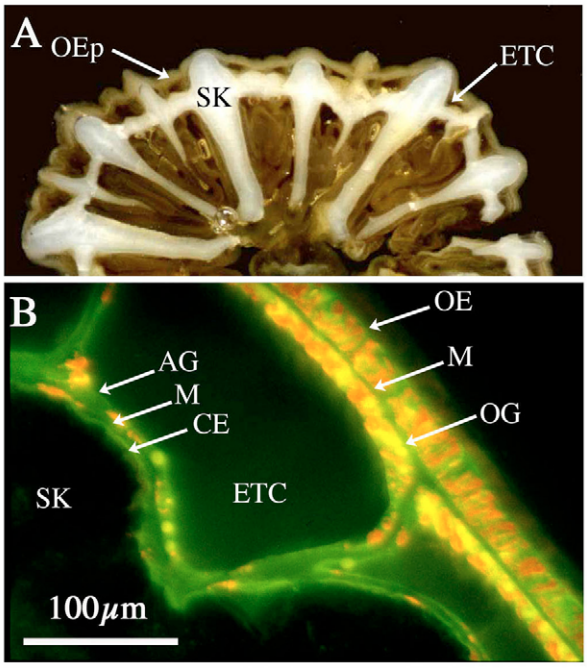

Fig. 1. (A) Transverse slice through a polyp of *Galaxea fascicularis* showing the oral epithelia (OEp) in relation to the skeleton (SK) and extrathecal coelenteron (ETC). (B) Fluorescence image of the extrathecal epithelia in a transverse slice of freeze-substituted *G. fascicularis* polyp. OE, oral ectoderm; M, mesogloea; OG, oral gastrodermis; ETC, extrathecal coelenteron; AG, aboral gastrodermis; CE, calicoblastic ectoderm; SK, skeleton.

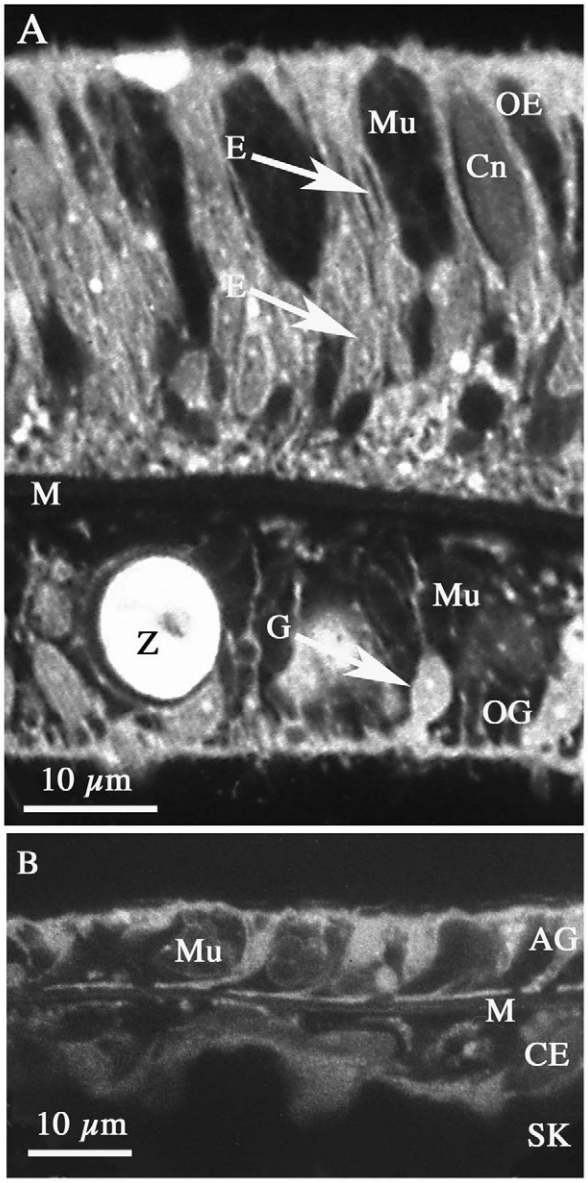

Fig. 2. Confocal images of a transverse slice (1 mm) of freeze-substituted *Galaxea fascicularis* showing (A) oral ectoderm (OE) and oral gastrodermis (OG) separated by mesogloea (M). In the OE, non-specialised ectoderm cells (E), mucocytes (Mu) and cnidocytes (Cn) are easily identified. The OG comprises non-specialised gastrodermis cells (G), mucocytes and zooxanthellae (Z). (B) The aboral epithelia consist of the aboral gastrodermis (AG), which is separated from the calicoblastic ectoderm (CE). Few zooxanthellae are present in the aboral gastrodermis and the epithelium consists primarily of mucocytes and non-specialised gastrodermis cells. The calicoblastic ectoderm consists of thin elongated cells containing numerous vesicles. Mucocytes are occasionally present. SK, skeleton.

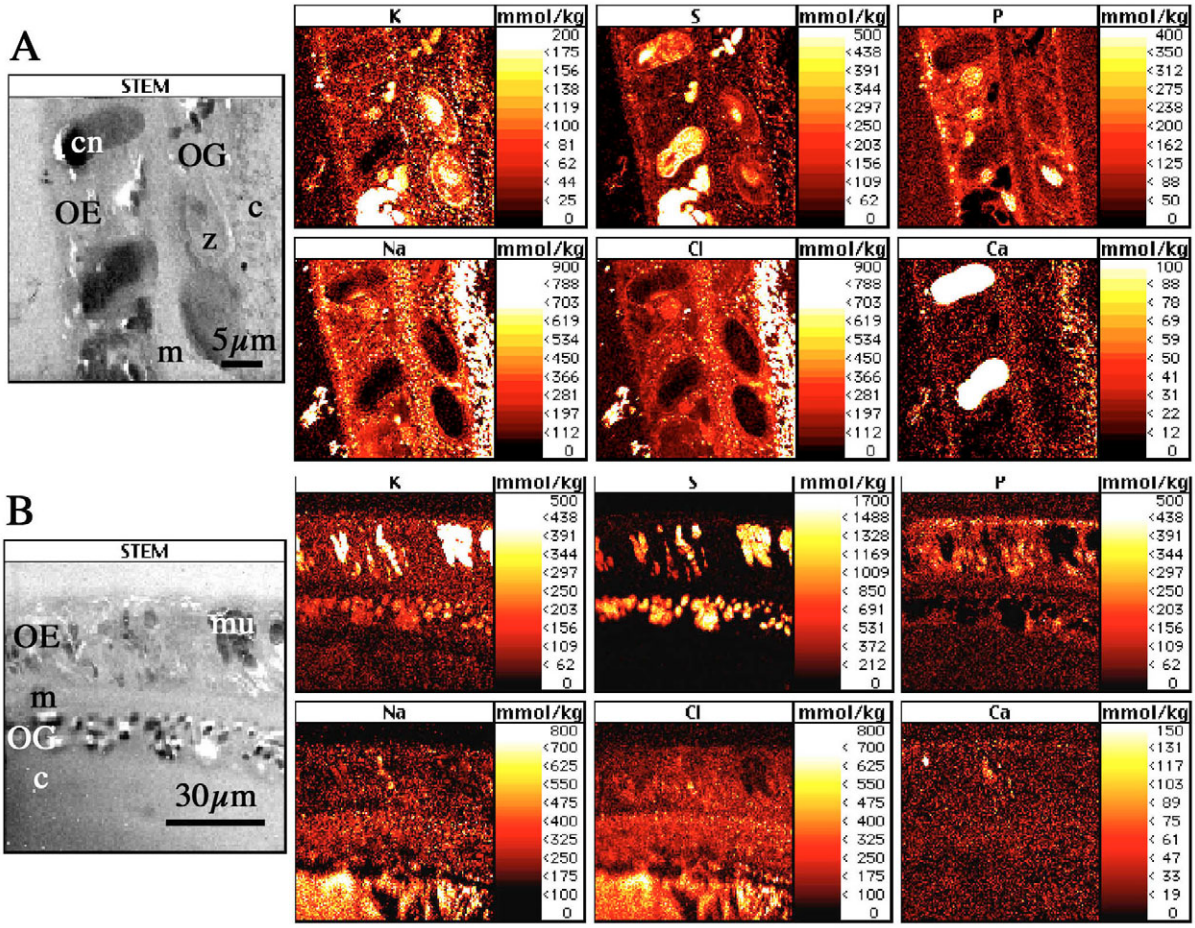

Fig. 3. STEM images of 1 μm-thick, freeze-substituted sections of *Galaxea fascicularis* showing typical regions of the oral epithelia. (A) The oral ectoderm (OE), containing dense cnidocytes (cn), is separated from the oral gastrodermis (OG) by the mesogloea (m). Two zooxanthellae (z) are present in the OG, and a part of the extrathecal coelenteron (c) is also shown. (B) The OE and OG are shown, containing numerous dense mucocytes (mu). Part of the extrathecal coelenteron is also shown. Elemental images of Na, Cl, P, S, K and Ca are shown, with the concentration of each element represented by a thermal colour scale (in mmol kg^{-1}). The Cl and Na images indicate the presence of NaCl in the extrathecal coelenteron and mesogloea.

X-ray microanalysis

Measurements of total Ca concentration were obtained from quantitative x-ray images derived from 1–2 μm-thick sections of freeze-substituted coral tissues (Fig. 3A,B). Potassium, Na, Cl, P and S images were obtained simultaneously to assist in the interpretation of Ca images and the identification of cellular regions and seawater compartments. The elemental concentrations differ slightly in the two sets of images but are within the range measured in this study.

In Fig. 3A,B it can be seen that high concentrations of Na and Cl were present in the seawater-filled space of the extrathecal coelenteron, indicating the retention of diffusible ions during the freeze-substitution process. Calcium concentration was high in cnidocysts and was clearly higher in the mesogloea and extrathecal coelenteron than in the coral cells and zooxanthellae. Calcium was frequently also in high concentration in mucocytes, particularly in the oral gastrodermis (Fig. 4).

In the aboral epithelium, the mesogloea was too thin to permit accurate analytical information to be extracted from x-ray images. Calcium concentrations were obtained from the aboral gastrodermis and calicoblastic ectoderm (Fig. 5). On the skeletal side of the calicoblastic ectoderm, loci of high Ca concentration are believed to represent nucleating calcium carbonate deposits on the organic matrix (Fig. 5). Fig. 5 also confirms the presence of NaCl in the sub-skeletal space.

Regions of interest were applied to images such as those in Fig. 3 to extract Ca concentrations from non-specialised epithelial cells and seawater-filled compartments (Fig. 6A,B). The Ca concentration in the mucus-containing external seawater layer was 21±5 mmol l^{-1} (mean ± s.e.m., n=3 where n is the number of measurements from one preparation). Because of the few data points, the calcium concentration of the latter compartment is not included in the statistical analysis in Fig. 6A.

Ion microprobe (SIMS) analysis

The distribution of C in secondary ion images of ^{12}C was homogeneous across the resin-embedded tissue and pure resin,

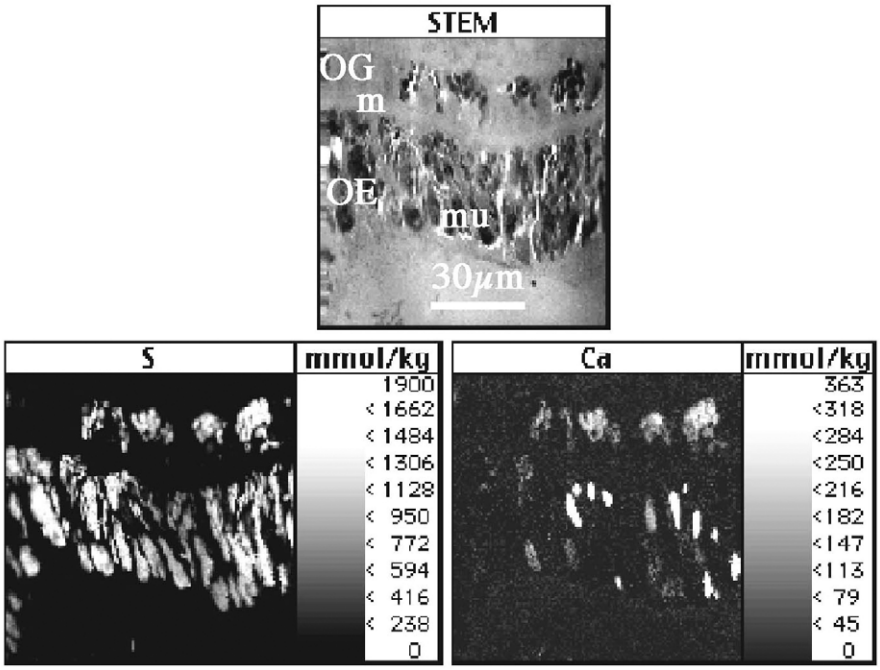

Fig. 4. STEM image of a 1 μm-thick, freeze-substituted section of *Galaxea fascicularis* showing the oral ectoderm (OE), mesogloea (m) and oral gastrodermis (OG). Elemental images of S and Ca are shown with concentrations (in mmol kg^{-1}) represented by a grey scale. Numerous S- and Ca-containing mucocytes (mu) are present in the oral ectoderm and gastrodermis.

indicating that local matrix effects on ion sputtering were minimal. The distribution of an elemental isotope in the SIMS images may thus be taken as an indication of relative concentration. The natural $^{44}Ca/^{40}Ca$ ratio (i.e. not enriched) is 0.02, thus any measure above this level is indicative of ^{44}Ca enrichment.

After 1 min exposure to ^{44}Ca, the tracer can be seen to have penetrated the oral epithelium and entered the extrathecal coelenteron (Fig. 7). However, the tracer did not appear to have entered the cells of the aboral epithelia. The $^{44}Ca/^{40}Ca$ ratio image and a line plot across this image (Fig. 7C,E) show that ^{44}Ca exceeds ^{40}Ca to a significant extent only in the external seawater layer after 1 min exposure.

After 8 min exposure to ^{44}Ca in the light, the tracer was present at higher levels in the mesogloea and extrathecal coelenteron than in the external seawater (Fig. 8B) and this is also reflected in the $^{44}Ca/^{40}Ca$ image and line scan (Fig. 8C,D). Very little ^{44}Ca appeared to have entered the aboral epithelia after 8 min and it was not present in the skeletal fragments adhering to the aboral epithelium.

After incubation for 8 min in the dark, a similar distribution of ^{44}Ca was apparent (Fig. 9) but the amount of ^{44}Ca relative to ^{40}Ca in the extrathecal coelenteron was lower in the dark than in the light [light, 1.38±0.14 (mean ± s.e.m.); dark, 0.75±0.29; N=3, P<0.05, where N represents the number of polyps].

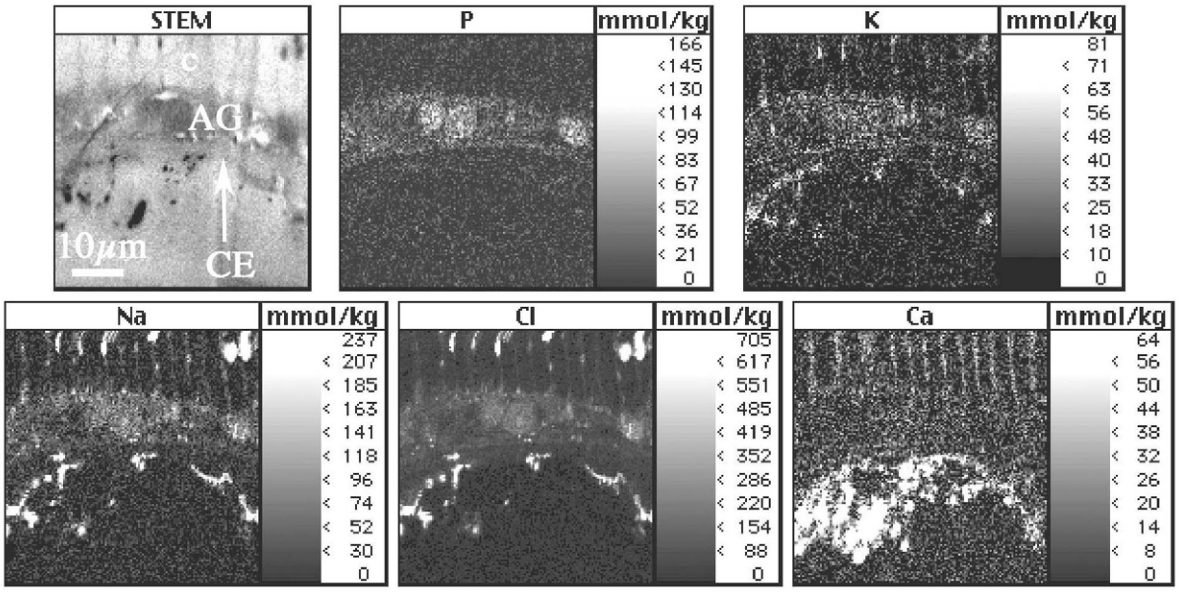

Fig. 5. STEM image of a 1 μm-thick, freeze-substituted section of *Galaxea fascicularis* showing part of the extrathecal coelenteron (c), aboral gastrodermis (AG) and calicoblastic ectoderm (CE). Elemental images of Na, Cl, P, K and Ca are shown with the concentration (in mmol kg^{-1}) of each element represented by a grey scale. The Ca image shows the presence of loci of nucleating calcium carbonate deposits on the organic matrix.

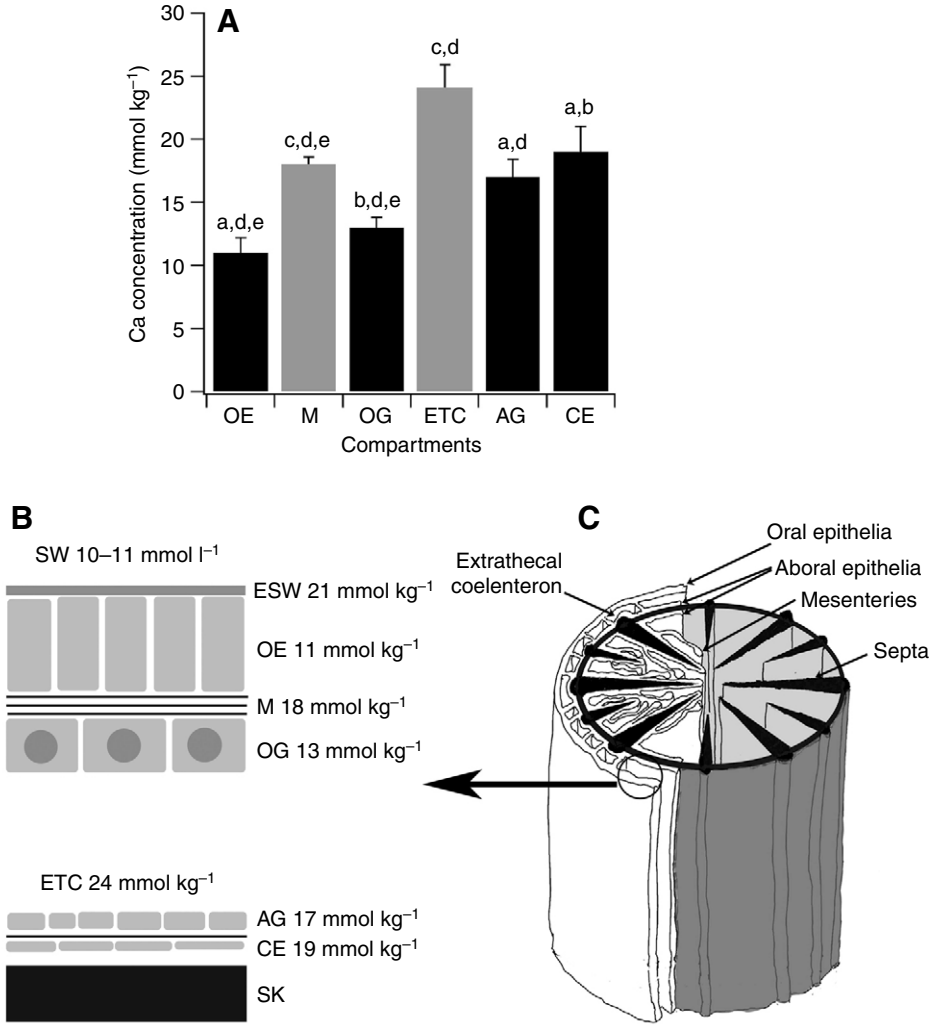

Fig. 6. (A) Concentrations of Ca (means ± s.e.m.) in the cells of the oral ectoderm (OE; *n*=60, *N*=6), mesogloea (M; *n*=37, *N*=4), cells of the oral gastrodermis (OG; *n*=51, *N*=5), extrathecal coelenteron (ETC; *n*=37, *N*=5), cells of the aboral gastrodermis (AG; *n*=34, *N*=3) and calicoblastic ectoderm (CE; *n*=33, *N*=3). *N* = number of polyps, *n* = number of measurements. Cellular compartments are represented by black bars and non-cellular compartments by grey bars. Values labelled with the same letter are significantly different ($P<0.05$). (B) Schematic diagram of coral epithelia showing Ca concentrations, as measured by x-ray microanalysis of freeze-substituted sections, in the external seawater layer (ESW), oral ectoderm (OE), mesogloea (M), oral gastrodermis (OG), extrathecal coelenteron (ETC), aboral gastrodermis (AG) and calicoblastic ectoderm (CE) adjacent to the skeleton (SK). Bulk seawater concentration (SW) is from Marshall and Clode (Marshall and Clode, 2003). (C) Cutaway diagram of a *Galaxea fascicularis* polyp, sectioned proximal to the mouth and tentacles, showing the organization of the extrathecal coelenteron compartments. The skeleton is shown in black. The data shown in A and summarised in B are from regions such as that shown in the circle in C.

High-resolution ion microprobe (NanoSIMS) analysis

Samples exposed to artificial SW containing ^{44}Ca for 1 min (i.e. from the same specimen as in Fig. 7) were analysed at the higher resolution offered by NanoSIMS. It can be seen (Fig. 10) that ^{44}Ca had entered the oral ectodermal cells and replaced a significant fraction of the original intracellular ^{40}Ca (Table 1). However, very little exchange had occurred in the mucocytes or cnidocytes, which contained considerably higher concentrations of ^{40}Ca than the unspecialised ectodermal cells. The $^{44}Ca/^{40}Ca$ ratio was higher in the mesogloea and slightly lower in the oral gastrodermal cells (Table 1), compared with the unspecialised ectodermal cells, and was extremely low in the zooxanthellae in the oral gastrodermis.

Analysis by NanoSIMS after 8 min exposure to ^{44}Ca showed that the $^{44}Ca/^{40}Ca$ ratio in the unspecialised ectodermal cells was only slightly higher than in the 1 min samples, but the ratios in the mesogloea and gastrodermal cells were considerably higher (Fig. 11; Table 1). Again, little exchange had occurred in the cnidocytes, mucocytes or zooxanthellae (Fig. 11).

Discussion

X-ray microanalysis showed that there is a gradient in total calcium, increasing from the outer oral epithelia to the inner aboral epithelia. The concentration rises from approximately 11 mmol kg^{-1} in the oral ectodermal cells to approximately 19 mmol kg^{-1} in the calicoblastic ectodermal cells.

Table 1. *Ratio of $^{44}Ca/^{40}Ca$ in cells and compartments of Galaxea polyps exposed to artificial seawater containing ^{44}Ca*

Time in ^{44}Ca (min)	Oral ectoderm	Mesogloea	Oral gastrodermis	Extrathecal coelenteron
1	0.44±0.03 (9)	0.54±0.01 (5)	0.35±0.01 (5)	0.26±0.01 (5)
8	0.52±0.05 (9)	1.49±0.09 (6)	1.11±0.05 (6)	1.59±0.17 (7)

Values are ratios ± s.e.m. (*N*=number of measurements from 3 polyps at each time interval).

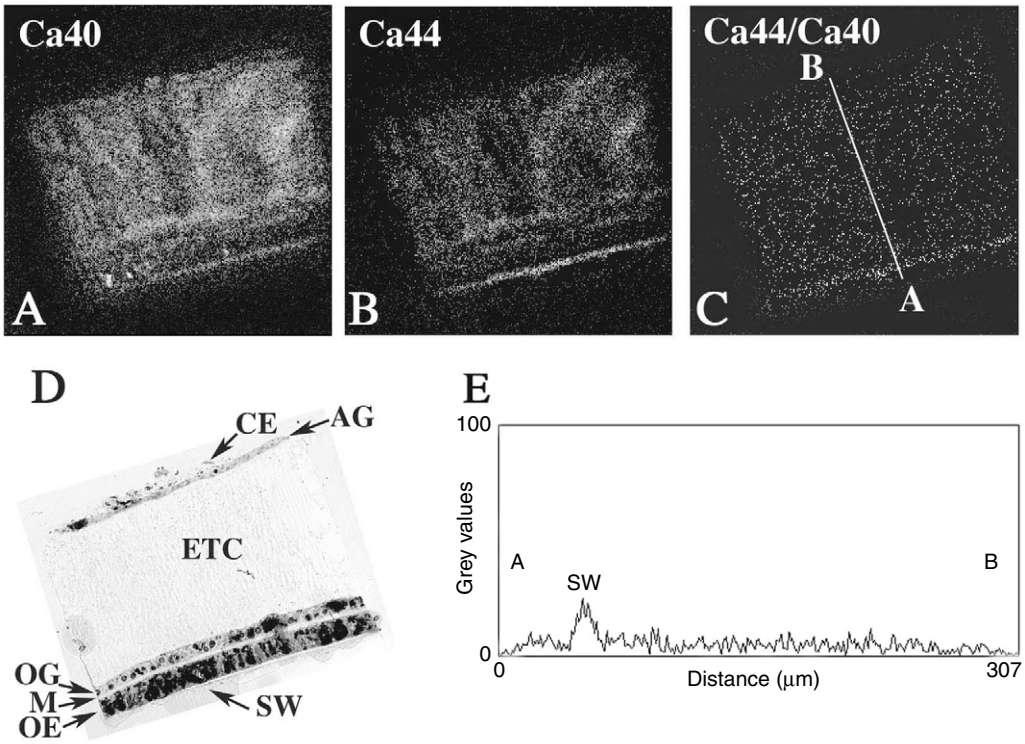

Fig. 7. Low spatial resolution SIMS images of a 2 μm-thick, freeze-substituted section of *Galaxea fascicularis* showing the distribution of (A) ^{40}Ca and (B) ^{44}Ca after 1 min incubation in ^{44}Ca artificial seawater in the light. The ^{44}Ca/^{40}Ca ratio image (C) and line profile (E) measured over A–B in (C) indicate that relatively little ^{44}Ca had entered the cells and extrathecal coelenteron, with the highest relative concentration being in the external seawater layer. Grey values in E represent pixel intensity values along A–B in (C) as a function of distance (μm). (D) Adjacent section, stained with Toluidine Blue, showing the external seawater layer (SW), oral ectoderm (OE), mesogloea (M), oral gastrodermis (OG), extrathecal coelenteron (ETC), aboral gastrodermis (AG) and calicoblastic ectoderm (CE).

Furthermore, calcium concentration in the mesogloea of the oral epithelium approaches 18 mmol kg^{-1}. These values are similar to those observed in settled larvae of *Pocillopora damicornis* (Clode and Marshall, 2004). The concentrations are recorded as mmol kg^{-1} embedded mass. This approximates to wet mass if the embedding resin replaces water. The total intracellular concentration of calcium in coral cells is high in comparison to the few measurements of total intracellular calcium concentration available for animal cells. In some terrestrial invertebrate tissues calcium concentrations have

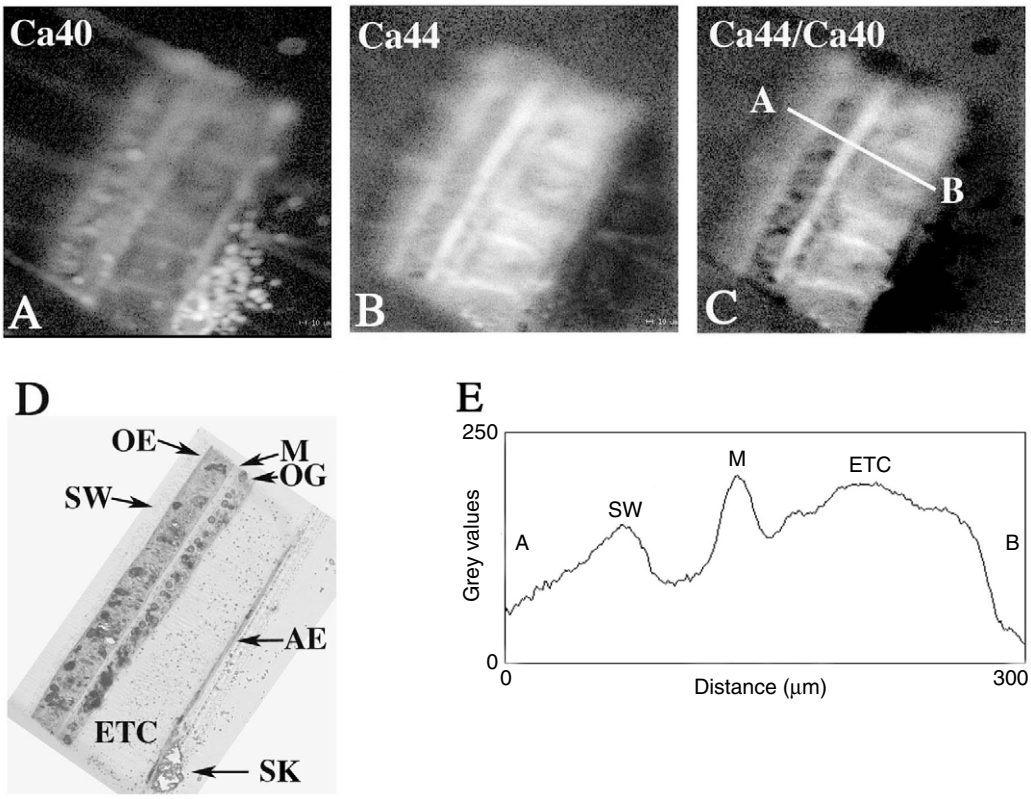

Fig. 8. Low spatial resolution SIMS images of a 2 μm-thick, freeze-substituted section of *Galaxea fascicularis* showing the distribution of (A) ^{40}Ca and (B) ^{44}Ca after 8 min incubation in ^{44}Ca artificial seawater in the light. The ^{44}Ca/^{40}Ca ratio image (C) and line profile (E) measured over A–B in (C) indicate that ^{44}Ca has reached a higher relative concentration in the mesogloea and extrathecal coelenteron than in the external seawater layer. Grey values in E represent pixel intensity values along A–B in (C) as a function of distance (μm). (D) Adjacent section, stained with Toluidine Blue, showing external seawater layer (SW), oral ectoderm (OE), mesogloea (M), oral gastrodermis (OG), extrathecal coelenteron (ETC), epithelia (AE) and skeleton (SK).

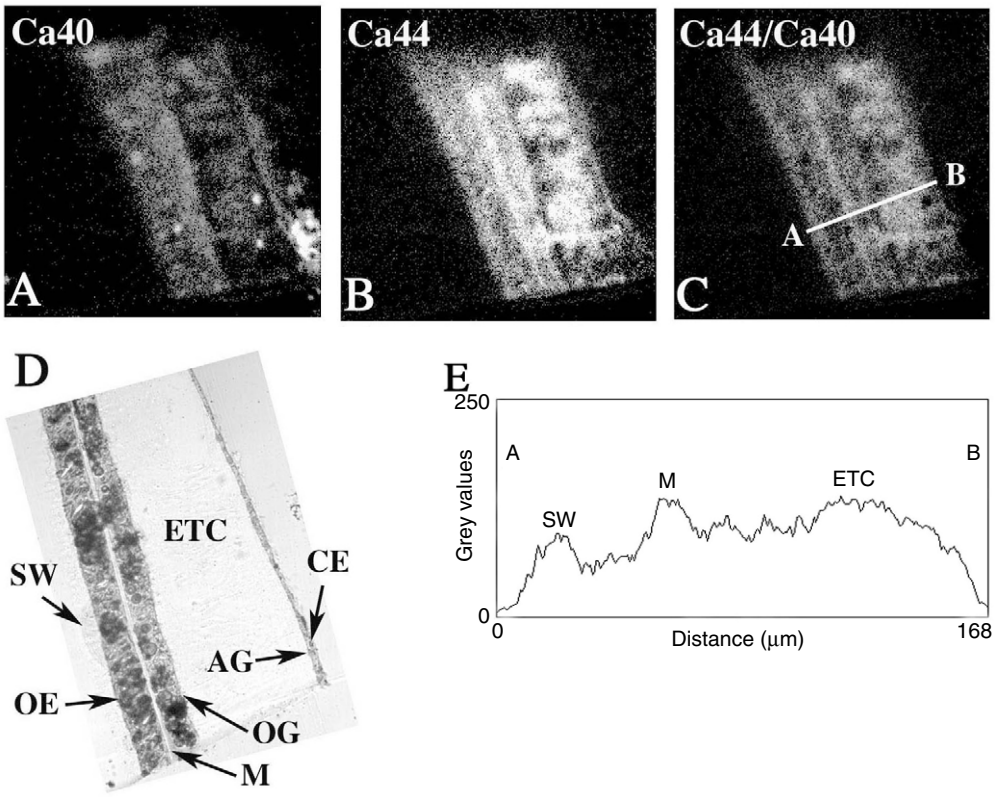

Fig. 9. Low spatial resolution SIMS images of a 2 μm-thick, freeze-substituted section of *Galaxea fascicularis* showing the distribution of (A) ^{40}Ca and (B) ^{44}Ca after 8 min incubation in Ca^{44} artificial seawater in the dark. The $^{44}Ca/^{40}Ca$ ratio image (C) and line profile (E) measured over A–B in (C) indicate that ^{44}Ca has reached a higher relative concentration in the mesogloea and extrathecal coelenteron than in the external seawater layer. The grey values, however, are lower than in Fig. 7. Grey values in E represent pixel intensity values along A–B in (C) as a function of distance (μm). (D) Adjacent section, stained with Toluidine Blue, showing the external seawater layer (SW), oral ectoderm (OE), mesogloea (M), oral gastrodermis (OG), extrathecal coelenteron (ETC), aboral gastrodermis (AG) and calicoblastic ectoderm (CE).

been recorded at less than 5 mmol kg^{-1} wet mass (reviewed by Gupta, 1993), although a concentration of 9 mmol kg^{-1} wet mass has been reported for the cytoplasm of nematoblast cells in an anemone (Lubbock et al., 1981). Our values are considerably higher than the estimate of 2.8 mmol l^{-1} derived from ^{45}Ca compartment analysis in *Stylophora pistillata* (Tambutté et al., 1996).

The gradient in total intracellular calcium concentration, increasing from the oral ectoderm in contact with seawater to the calicoblastic ectoderm in contact with the skeleton, suggests that a pool of intracellular calcium is accumulated for deposition in the skeleton. The high concentration of calcium in the mesogloea of the oral epithelium suggests that this compartment has some role in the transport of Ca^{2+} across the epithelium. Unfortunately, the dimensions of the mesogloea of the aboral epithelium were too small to permit measurement of calcium concentration.

In an x-ray microanalystical study of frozen-hydrated *Galaxea* polyps, Clode and Marshall found that the calcium concentration in the extrathecal coelenteron (22 mmol kg^{-1} wet mass) was significantly higher than in the mucus-containing seawater (16 mmol kg^{-1} wet mass) (Clode and Marshall, 2002a). The latter was, in turn, significantly higher

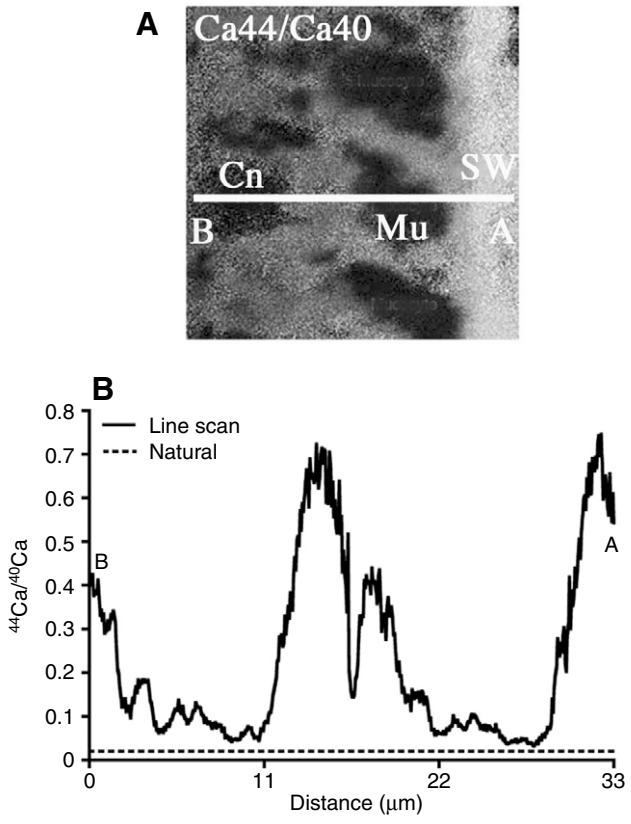

Fig. 10. High-resolution NanoSIMS image of a 2 μm-thick, freeze-substituted section of *Galaxea fascicularis* after 1 min incubation in ^{44}Ca artificial seawater in the light. The $^{44}Ca/^{40}Ca$ ratio image (A) and line profile (B) indicate that ^{44}Ca had reached a high relative concentration in the unspecialised oral ectodermal cells but little exchange had occurred in the mucocytes (Mu) or cnidocytes (Cn). Natural (unenriched) levels are also indicated. SW, external seawater layer. In B the ratio $^{44}Ca/^{40}Ca$ along B–A in (A) is plotted against distance (μm).

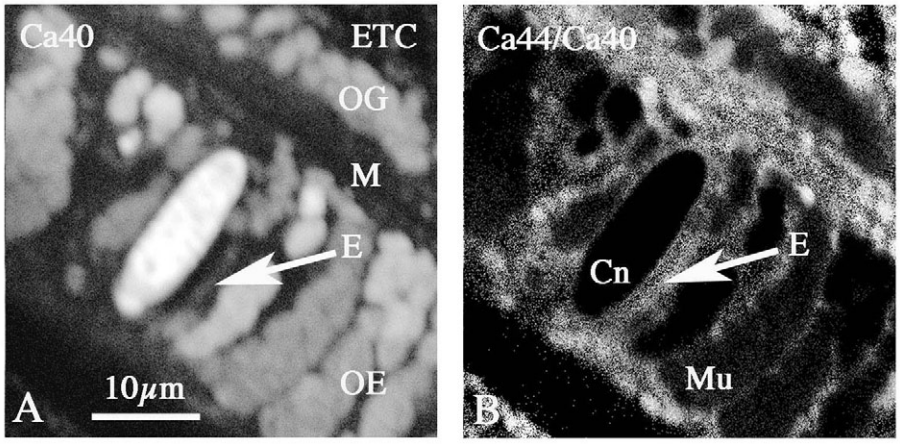

Fig. 11. High-resolution NanoSIMS image of a 2 μm-thick, freeze-substituted section of *Galaxea fascicularis* after 8 min incubation in ^{44}Ca artificial seawater in the light. The ^{40}Ca image (A) shows very high levels of ^{40}Ca in cnidocytes and mucocytes in the oral ectoderm (OE) and oral gastrodermis (OG) compared with unspecialised ectodermal cells (E) and mesogloea (M). ETC, extrathecal coelenteron. The $^{44}Ca/^{40}Ca$ ratio image (B) indicates that ^{44}Ca had reached a high relative concentration in the unspecialised oral ectodermal cells (E) and mesogloea but relatively little exchange had occurred in the mucocytes (Mu) or cnidocytes (Cn).

than in the bulk seawater (12 mmol kg^{-1}). These data suggested that active transport of calcium may occur across the oral epithelium. Our present data are consistent with this view. In freeze-substituted sections of *Galaxea* polyps, the calcium concentration in the extrathecal coelenteron was 24 mmol kg^{-1} embedded mass. In the mucus-containing external seawater layer, the calcium concentration was 21 mmol kg^{-1} embedded mass. The latter was based on only three acceptable measurements and may not be a reliable estimate. However, the trend is similar to that observed in the analyses of frozen-hydrated polyps. Measurement by ion-selective electrodes (Marshall and Clode, 2003) indicates that the concentration of unbound calcium in this layer is 14.5 mmol l^{-1}, i.e. slightly lower than the concentration measured in frozen-hydrated polyps. The pattern of calcium distribution across the epithelia, mesogloea and extrathecal coelenteron is very similar to that seen in settled larvae of *Pocillopora damicornis* (Clode and Marshall, 2004).

These data indicate that Ca^{2+} is being transported across the oral epithelia against a concentration gradient. If transport occurs in the absence of an electrical gradient or against an electrochemical gradient then the process is likely to be an active one requiring energy. There are no *in vivo* measurements of transepithelial potentials in *Galaxea* or in any other corals as far as we are aware. However, transepithelial potentials of isolated preparations of oral epithelia of *Lobophyllia hemprichii* and *Plerogyra sinuosa* in Ussing chambers were less than 1 mV (gastrodermal side negative to the ectodermal side) (Wright and Marshall, 1991). These preparations exhibited a net flux of Ca^{2+} from the ectodermal side to the gastrodermal side. It seems possible, therefore, that Ca^{2+} is transported against a concentration gradient in the absence of a significant electrical gradient in intact polyps.

It is possible that a favourable transepithelial potential for Ca^{2+} entry could be generated in intact polyps by the release into the extrathecal coelenteron of OH^- from the photosynthesising zooxanthellae found in the oral and aboral gastrodermis. Certainly, pH in the coelenteron proper does increase when polyps are illuminated (A.T.M. and P.L.C., unpublished data). However, this mechanism seems unlikely because a high calcium concentration is maintained in the extrathecal coelenteron under dark conditions when photosynthesis is not occurring (Clode and Marshall, 2002a).

Scleractinian corals transport prodigious quantities of Ca from seawater for incorporation into the $CaCO_3$ skeleton. Wright and Marshall measured net Ca^{2+} flux through isolated coral epithelia in Ussing chamber experiments at 1.1 μmol cm^{-2} h^{-1} (Wright and Marshall, 1991). Making some simple assumptions about polyp dimensions, it can be calculated from data on skeletal ^{45}Ca incorporation (Marshall, 1996; Marshall and Clode, 2004) that Ca^{2+} flux is 4.8–9.6 μmol cm^{-2} h^{-1}. These values compare reasonably well with estimates of 1.7 μmol cm^{-2} h^{-1} Ca^{2+} flux in *Acropora* (Wilbur and Simkiss, 1979). Using the calculated flux data and estimates of the volume of the extrathecal coelenteron from measurements made on slices of freeze-substituted *Galaxea* polyps, it can be shown that the Ca^{2+} content of the extrathecal coelenteron would be removed in 6–12 min in the light and in 22–45 min in the dark if no further Ca^{2+} entry occurred. These calculations are consistent with the observations of ^{44}Ca tracer entry in light and dark conditions. After incubation for 8 min in the light, ^{44}Ca had almost replaced ^{40}Ca in the external coelenteron whereas this was not the case in the dark. Very little exchange in the extrathecal coelenteron had occurred after 1 min.

After 8 min incubation in ^{44}Ca in the light, ^{40}Ca had almost completely been replaced by ^{44}Ca in the mucus-containing layer of external seawater, but the concentration of ^{44}Ca in the extrathecal coelenteron was higher, as shown in the $^{44}Ca/^{40}Ca$ ratio image and line scan. In the absence of a favourable transepithelial potential this could only be a consequence of some sort of active Ca^{2+} transport across the oral epithelium.

Analysis of samples incubated for 1 min and 8 min in ^{44}Ca by NanoSIMS showed clearly that Ca^{2+} rapidly entered the oral ectodermal cells and exchanged with approximately 30% of the total cell calcium. After 8 min incubation, the fraction of calcium exchanged in the ectodermal cells had risen only slightly to 33%. Thus, in these cells there is both a rapidly exchanging pool and a large slowly exchanging pool of Ca. This is consistent with the observations of Marshall and Wright, who observed a slowly exchanging Ca pool in the

tissues by ^{45}Ca autoradiography (Marshall and Wright, 1998). In the mesogloea and the gastrodermal cells, the amount of Ca exchanged after 8 min was approximately 60 and 53%, respectively. The transport of Ca^{2+} appears to be principally transcellular in both the oral ectoderm and gastrodermis.

The uptake of ^{45}Ca by the skeleton has been shown to be inhibited by Ruthenium Red (Krishnaveni et al., 1989; Marshall, 1996). This has been interpreted as evidence of the presence of a Ca-ATPase in coral tissues. *In situ* hybridization evidence indicates that this ATPase is principally located in the calicoblastic cells but is also present in the aboral and oral gastrodermal cells but not in the oral ectoderm (Zoccola et al., 2004). Thus, active transport of Ca^{2+} is thought to occur at the skeletal face of the calicoblastic cells, as proposed by McConnaughey (McConnaughey, 1994). Evidence of an active transport mechanism in the oral epithelium has been derived from Ussing chamber experiments (Wright and Marshall, 1991), while evidence based on x-ray microanalysis has been described by Clode and Marshall (Clode and Marshall, 2002a). However, Ca-ATPase may not be the conduit for active transport of Ca^{2+} across the oral epithelium because light-activated uptake of Ca^{2+} at the surface of the oral ectoderm in zooxanthellate corals is not inhibited by the Ca-ATPase inhibitor Ruthenium Red (Marshall and Clode, 2003).

It seems probable that the oral mesogloea is involved in the transport of Ca^{2+} across the oral epithelium because total Ca in this compartment is high and ^{40}Ca is rapidly exchanged for ^{44}Ca; the mechanism, however, is obscure. In anemones, the mesogloea appears to be composed of collagen fibrils within an amorphous matrix that is composed of neutral protein–polysaccharide complexes (Gosline, 1971a; Gosline, 1971b; Koehl, 1973; Young, 1973). In *Galaxea*, the mesogloea is bounded by membrane-like structures (Clode and Marshall, 2002b) that are distinct from the adjacent cell membranes. These may be formed from laminins, as occur at the subepithelial boundaries of *Hydra* mesogloea (Sarras and Deutzmann, 2001). Although some charge shielding by inorganic cations may occur in the mesogloea of the anemone *Metridium senile* (Gosline, 1971a) to reduce electrostatic interactions between collagen and the matrix complexes, the number of charged sites is considered to be small. Our analysis of mesogloea in *Galaxea* indicates an increased Ca concentration compared with seawater. In the absence of extensive polyanionic charges, it seems unlikely that the increased Ca concentration is due to electrostatic interactions. It is interesting to note that Macklin, using autoradiography, found that calcium accumulated in high concentration in the mesogloea of *Hydra* and suggested that this accumulation resulted from active transport across the ectoderm (Macklin, 1967).

The data show that an intracellular concentration gradient for total calcium exists across the outer and inner epithelia of *Galaxea* polyps. The gradient increases from the oral ectoderm to the calicoblastic ectoderm. Based on data from the present investigation and previous studies (Clode and Marshall, 2002a; Marshall and Clode, 2003; Clode and Marshall, 2004), there is also an increasing calcium gradient from bulk seawater to the mucus-containing external seawater layer, mesogloea and extrathecal coelenteron. The data also indicate that Ca^{2+} transport across the oral epithelium is transcellular and that entry into the extrathecal coelenteron is against a concentration gradient, possibly by some active transport process. Furthermore, the mesogloea is involved in this process. The movement of Ca^{2+} across the oral epithelium is initiated by light and is proportional to light intensity (Marshall and Clode, 2003). Thus, it is not surprising that the extrathecal coelenteron $^{44}Ca/^{40}Ca$ ratio measured in polyps incubated in the dark is lower than that measured in the light. This appears to be further evidence against paracellular Ca^{2+} transport since it would be expected that the ratio would be similar in light and dark conditions if Ca^{2+} transport occurred by passive paracellular diffusion.

A possible explanation for the occurrence of active transcellular Ca^{2+} transport into the extrathecal coelenteron may be that the epithelium must be tight to prevent the dissipation of a proton gradient generated by the deposition of calcium carbonate at the skeletal surface. It is hypothesised that protons generated during the formation of calcium carbonate are exchanged for Ca^{2+} *via* a Ca-ATPase in the calicoblastic epithelial cells (McConnaughy and Whelan, 1997). The protons are transported into the fluid-filled coelenteron where they keep the pH of the coelenteron seawater low and the concentration of CO_2 high for the photosynthetic needs of the symbiotic algae (Cohen and McConnaughy, 2003). Alternatively, the protons may neutralise OH^- produced by the photosynthesis of intracellular symbiotic algae present primarily in the oral gastrodermis (Allemand et al., 2004). In *Galaxea*, calcification occurs principally on the outside of the thecal walls of the corallite (Marshall and Wright, 1998). Covering these walls are the inner aboral epithelia and the outer oral epithelia separated by the extrathecal coelenteron. The latter is divided into longitudinal compartments that have restricted continuity with the internal coelenteron (see Fig. 6C).

Within each compartment, fluid circulates by ciliary action, frequently in countercurrents in adjacent compartments (A.T.M. and P.L.C., unpublished data). Thus, these compartments are semi-isolated and receive protons from calcium carbonate deposition and possibly hydroxyl ions from algal photosynthesis. If these compartments are functionally isolated from the inner coelenteron then it is perhaps not surprising that some form of active Ca^{2+} transport should occur across the oral epithelium. As shown by the NanoSIMS analysis, the passage of ^{44}Ca across the epithelium appears to be transcellular.

This research was supported by AINSE grants to A.T.M. and UWA Research and NANO TAP grants to P.L.C. The Cameca NanoSIMS50 facility at The University of WA was funded by a Major National Research Facility (MNRF) grant through the Nanostructural Analysis Network Organisation (NANO). Corals were collected under Great Barrier Reef Marine Park Authority permits to A.T.M.

References

Allemand, D., Ferrier-Pagès, C., Furla, P., Houlbrèque, F., Puverel, S., Reynaud, S., Tambutté, E., Tambutté, S. and Zoccola, D. (2004). Biomineralisation in reef-building corals: from molecular mechanisms to environmental control. *C. R. Palevol* **3**, 453-467.

Benazet-Tambutté, S., Allemand, D. and Jaubert, J. (1996). Permeability of the oral epithelial layers in cnidarians. *Mar. Biol.* **126**, 43-53.

Bordat, C., Guerquin-Kern, J.-L., Lieberherr, M and Gournot, G. (2004). Direct visualization of intracellular calcium in rat osteoblasts by energy-filtering transmission electron microscopy. *Histochem. Cell Biol.* **121**, 131-138.

Brini, M. and Carafoli, E. (2000). Calcium signalling: a historical account, recent developments and future perspectives. *Cell. Mol. Life Sci.* **57**, 354-370.

Clode, P. L. and Marshall, A. T. (2002a). Low temperature x-ray microanalysis of calcium in a scleractinian coral: evidence of active transport mechanisms. *J. Exp. Biol.* **205**, 3543-3552.

Clode, P. L. and Marshall, A. T. (2002b). Low temperature FESEM of the calcifying interface of a scleractinian coral. *Tissue Cell* **34**, 187-189.

Clode, P. L. and Marshall, A. T. (2004). Calcium localisation by x-ray microanalysis and fluorescence microscopy in larvae of zooxanthellate and azooxanthellate corals. *Tissue Cell* **36**, 379-390.

Clode, P. L., Stern, R. and Marshall, A. T. (2007). Subcellular imaging of isotopically labeled carbon compounds in a biological sample by ion microprobe (NanoSIMS). *Microsc. Res. Tech.* **70**, 220-229.

Cohen, A. L. and McConnaughey, T. A. (2003). Geochemical perspectives on coral mineralization. *Rev. Min. Geochem.* **54**, 151-187.

Gosline, J. M. (1971a). Connective tissue mechanics of *Metridium senile*. 1. Structural and compositional aspects. *J. Exp. Biol.* **55**, 763-774.

Gosline, J. M. (1971b). Connective tissue mechanics of *Metridium senile*. 2. Visco-elastic properties and macromolecular model. *J. Exp. Biol.* **55**, 775-795.

Guerquin-Kern, J.-L., Wu, T.-D., Quintana, C. and Croisy, A. (2005). Progress in analytical imaging of the cell by dynamic secondary ion mass spectrometry (SIMS microscopy). *Biochim. Biophys. Acta* **1724**, 228-238.

Gupta, B. L. (1993). Electron probe x-ray microanalysis of diffusible ions in cells and tissues from invertebrate animals. In *X-ray Microanalysis in Biology: Experimental Techniques and Applications* (ed. D. C. Sigee, A. J. Morgan, A. T. Sumner and A. Worley), pp. 231-256. Cambridge: Cambridge University Press.

Hall, T. A. and Gupta, B. L. (1979). EDS quantitation and application to biology. In *Introduction to Analytical Electron Microscopy* (ed. J. J. Hren, J. J. Goldstein and D. C. Joy), pp. 169-197. New York: Plenum Press.

Hoenderop, J. G. J., Nilius, B. and Bindels, R. J. M. (2005). Calcium absorption across epithelia. *Physiol. Rev.* **85**, 373-423.

Ingram, P., Shelburne, J. D. and LeFurgey, A. (1999). Principles and instrumentation. In *Biomedical Applications of Microprobe Analysis* (ed. P. Ingram, J. D. Shelburne, V. L. Roggli and A. LeFurgy), pp. 1-57. San Diego: Academic Press.

Koehl, M. A. R. (1977). Mechanical diversity of connective tissue of the body wall of sea anemones. *J. Exp. Biol.* **69**, 107-125.

Krishnaveni, P., Chou, L. M. and Ip, Y. K. (1989). Deposition of calcium ($^{45}Ca^{2+}$) in the coral *Galaxea fascicularis*. *Comp. Biochem. Physiol.* **94A**, 509-513.

Lechene, C., Hillion, F., McMahon, G., Benson, D., Kleinfield, A. M., Kampf, J. P., Distel, D., Luyten, Y., Bonventre, J., Hentschel, D. et al. (2006). High resolution quantitative imaging of mammalian and bacterial cells using stable isotope mass spectrometry. *J. Biol*. **5**, 20-30.

LeFurgey, A., Davilla, S. D., Kopf, D. A., Somner, J. R. and Ingram, P. (1992). Real-time quantitative elemental analysis and mapping: microchemical imaging in cell physiology. *J. Microsc.* **165**, 191-223.

Lubbock, R., Gupta, B. L. and Hall, T. A. (1981). Novel role of calcium in exocytosis: mechanism of nematocyst discharge as shown by x-ray microanalysis. *Proc. Natl. Acad. Sci. USA* **78**, 3624-3628.

Macklin, M. (1967). Osmotic regulation in *Hydra*: sodium and calcium localization and source of electrical potential. *J. Cell. Physiol.* **70**, 191-196.

Marshall, A. T. (1980). Freeze-substitution as a preparative technique for biological x-ray microanalysis. *Scan. Electron Microsc.* **1980**, 395-408.

Marshall, A. T. (1996). Calcification in hermatypic and ahermatypic corals. *Science* **271**, 637-639.

Marshall, A. T. and Clode, P. L. (2003). Light regulated Ca^{2+} uptake and O_2 secretion at the surface of a scleractinian coral *Galaxea fascicularis. Comp. Biochem. Physiol.* **136A**, 417-426.

Marshall, A. T. and Clode, P. L. (2004). Calcification rate and the effect of temperature in a zooxanthellate and an azooxanthellate scleractinian reef coral. *Coral Reefs* **23**, 218-224.

Marshall, A. T. and Wright, A. (1998). Coral calcification: autoradiography of a scleractinian coral *Galaxea fascicularis* after incubation in ^{45}Ca and ^{14}C. *Coral Reefs* **17**, 37-47.

Marshall, A. T. and Wright, O. P. (1991). Freeze-substitution of scleractinian coral for confocal laser scanning microscopy and x-ray microanalysis. *J. Microsc.* **162**, 341-354.

McConnaughey, T. A. (1994). Calcification, photosynthesis and global carbon cycles. In *Past and Present Biomineralization Processes* (ed. F. Doumenge), pp. 137-162. Monaco: Museé Océanographique.

McConnaughey, T. A. and Whelan, J. F. (1997). Calcification generates protons for nutrient and bicarbonate uptake. *Earth Sci. Rev.* **42**, 95-117.

Pålsgård, E., Lindh, U. and Roomans, G. (1994). Comparative study of freeze-substitution techniques for x-ray microanalysis. *Microsc. Res. Tech.* **28**, 254-258.

Pozzan, T., Rizzuto, R., Volpe, P. and Meldolesi, J. (1994). Molecular and cellular physiology of intracellular calcium store. *Physiol. Rev.* **74**, 595-637.

Sarras, M. P. and Deutzmann, R. (2001). *Hydra* and Niccolo Paganini (1782–1840) – two peas in a pod? The molecular basis of extracellular matrix structure in the invertebrate, *Hydra*. *BioEssays* **23**, 716-724.

Tambutté, E., Allemand, D., Mueller, E. and Jaubert, J. (1996). A compartmental approach to the mechanism of calcification in hermatypic corals. *J. Exp. Biol.* **199**, 1029-1041.

Wilbur, K. M. and Simkiss, K. (1979). Carbonate turnover and deposition in metazoa. In *Studies in Environmental Science 3, Biogeochemical Cycling of Mineral-forming Elements* (ed. P. A. Trudinger and D. J. Swaine), pp. 69-106. Amsterdam: Elsevier.

Wright, O. P. and Marshall, A. T. (1991). Calcium transport across the isolated oral epithelium of scleractinian corals. *Coral Reefs* **10**, 37-40.

Young, S. D. (1973). Collagen and other mesoglea protein from the coral *Lobophyllia corymbose* (Anthozoa, Scleractinia). *Int. J. Biochem.* **4**, 339-344.

Zoccola, D., Tambutté, E., Kulhavek, E., Puverel, S., Scimeca, J.-C., Allemand, D. and Tambutté, S. (2004). Molecular cloning and localization of a PMCA P-type calcium ATPase from the coral *Styllophora pistillata*. *Biochim. Biophys. Acta* **1-2**, 117-126.